Applied Thermal Engineering 130 (2018) 1175–1181

Contents lists available at ScienceDirect

Applied Thermal Engineering

journal homepage: www.elsevier.com/locate/apthermeng

Research Paper

Raman thermometry analysis: Modelling assumptions revisited

Juliana Jaramillo-Fernandez [a,*], Emigdio Chavez-Angel [b], Clivia M. Sotomayor-Torres [b,c]

[a] Department of Applied Physics, KTH Royal Institute of Technology, Electrum 229, 164 40 Kista, Sweden
[b] Catalan Institute of Nanoscience and Nanotechnology (ICN2), CSIC and The Barcelona Institute of Science and Technology, Campus UAB, Bellaterra, 08193 Barcelona, Spain
[c] ICREA, Passeig Lluís Companys 23, 08010 Barcelona, Spain

HIGHLIGHTS

- The assumptions in the heat conduction models in Raman thermometry are revisited.
- Sources of errors from the modelling assumptions in Raman thermometry are analysed.
- Our results are a powerful tool to select appropriate samples for Raman thermometry.
- Our work serves to improve the accuracy of Raman thermometry measurements.

ARTICLE INFO

Article history:
Received 9 June 2017
Revised 13 September 2017
Accepted 5 November 2017
Available online 11 November 2017

2017 MSC:
00-01
99-00

Keywords:
Raman thermometry
Numerical modelling
Thermal conductivity
Bulk
Semiconductors

ABSTRACT

In Raman thermometry, several assumptions are made to model the heat conduction and to extract the thermal conductivity of the samples from the measured data. In this work, the heat conduction in bulk and mesa-like samples was investigated by numerical simulation and measured by the temperature-induced Raman shift method, to study the range of applicability of these assumptions. The effects of light penetration depth and finite sample size on the accuracy of the thermal conductivity determination were investigated by comparing the results of the finite element method with the usual analytical approximation for bulk samples. We found that the assumptions used in the analytical model can be applied to extract the thermal conductivity in solids if the following conditions are fulfilled: the ratio of light penetration depth to laser spot radius is smaller than 0.5, the ratio of spot radius to sample thickness is smaller than 0.1, and the ratio of spot radius to sample half width is smaller than 0.01.

1. Introduction

The accurate experimental determination of the thermal conductivity of bulk materials is a very challenging task. It usually involves the measurement of temperature differences across a sample in response to the introduction of thermal energy into the system [1,2]. In general, each thermal characterization technique is limited to a specific range of thermophysical properties, dimensions and geometry of the sample under analysis [3]. Therefore, the accuracy of the obtained thermal conductivity value depends upon the applicability of the measurement technique to a specific sample. Other factors that might influence the accuracy of the results are, for example, heat losses during the measurements and poorly controlled thermal contact resistances between the specimen and the sample holder.

Despite the experimental challenges, several electro- and optothermal methods for characterization of the thermal properties of a large variety of bulk materials are currently available [4–9]. Electrothermal methods generally use microfabricated metal lines to induce Joule heating and probe temperature changes based on the temperature-dependent electrical resistance of the metal strip. Alternatively, optothermal techniques use laser light as a heat source and measuring probe. The latter approaches are advantageous over electrothermal techniques because they forestall the need for electrical contacts, facilitating measurements in vacuum.

One contactless non-destructive optical method to measure the thermal conductivity of bulk materials is Raman thermometry. In recent years, this technique has gained popularity [10–17], mainly because it offers sub-micrometer spatial resolution and high sensitivity to temperature, given by the Gaussian laser beam size and

* Corresponding author.
E-mail address: jjf@kth.se (J. Jaramillo-Fernandez).

https://doi.org/10.1016/j.applthermaleng.2017.11.033
1359-4311/

the temperature-dependent Raman shift of any of the active optical phonon modes of the studied material [18,19]. In Raman thermometry, a focused laser beam is used as the heat source, and the temperature dependence of an active Raman mode acts as the thermometer, provided that it has a sufficiently large spectral shift as a function of temperature [20]. The heating induced by the Gaussian laser beam results in a non-homogeneous temperature field in the excited region of the sample. Therefore, the effective temperature rise, derived from the collected Raman spectra, is an average of the temperature weighted over the probed volume [21,22]. The experimental data of weighted temperature as a function of the power absorbed in the probed volume are then compared to a heat conduction model to extract the thermal conductivity. In the case of bulk materials and thick layers, an analytical expression based on the steady-state two-dimensional heat conduction equation solved for a Gaussian heat source is generally used [23–25,13,26,21]. In this derivation, the material under study is considered as a semi-infinite medium with strong light absorption at the surface. However, sometimes samples may differ from these ideal cases: they may not be considered as semi-infinite nor have shallow light penetration depth at the used laser wavelength. Under either or both of these experimental conditions, to make such assumptions in the analysis of the data may introduce considerable measurement errors.

To date, few studies have addressed error sources in laser Raman thermometry. In a recent work, Stoib and co-workers [21] highlighted the need to consider the non-uniform temperature distribution resulting from the laser excitation to interpret correctly the effective temperature extracted from Raman spectra. Moreover, Beechem et al. [27] studied the error and uncertainty emerging from inconsistencies in the thermal models used to extract the thermal conductivity, uncertainties in the measured parameters such as temperature and heat input, as well as the biasing that occurs due to thermo-mechanical stress. In addition, they showed that for most materials, the assumption of a "temperature-independent thermal conductivity" can yield to errors between 5% and 10%. In a previous work [28], the authors also analysed several spectral features that can be used to measure the sample temperature, including the position, linewidth, and intensity of the Raman signal. They considered the practical application of the method using each of these spectral characteristics and demonstrated that each of them offers particular advantages depending on the studied specimen. Despite these recent efforts, the constrains and ranges of validity where the simplified analytical model applies, are not well documented in the literature.

In this work, a finite element simulation of the heating of a bulk sample by a Gaussian laser beam is presented. The validity ranges of the assumptions involved in the heat conduction model were evaluated. Bulk Ge and InP were chosen as representative samples to study the role of the light penetration depth. Experimental data for bulk Si measured by Stoib and colleagues [21] were also analysed using our numerical model. Furthermore, to investigate the finite size effects, InP microcrystals were analysed. By comparing our numerical model with the simplified analytical solution for the case of laser heating of a semi-infinite solid, we obtained the range of applicability of different conditions, such as sample dimensions and penetration depth of light in the studied material. The modelling results were validated by Raman thermal conductivity experiments.

2. Modelling of the temperature field

2.1. Radial analytical approximation

The Raman shift method is often used in thermometry to characterize the thermal conductivity of bulk materials using a simple two-dimensional heat conduction model [21,25,24]. In the case of a Gaussian laser beam heating the surface of a semi-infinite medium defined in the $x-z$ plane, the induced temperature rise can be calculated by solving the steady-state heat equation given by:

$$-\kappa\nabla^2 T = \frac{2P_a}{\pi r^2}\exp\left[-2\frac{x^2}{r^2}\right] \tag{1}$$

where P_a is the power absorbed at the surface, κ is the thermal conductivity of the material, and r is the laser spot radius. This two-dimensional heat conduction problem was first solved by Carslaw and Jaeger [29]. Considering that the excitation power is strongly absorbed at the surface of an isotropic and semi-infinite material, so that the induced distribution of isotherms is hemispherical, the thermal conductivity is constant and the convection and radiation losses are negligible, an analytical linear solution can be derived from Eq. (1):

$$\Delta T = \frac{P_a}{4\sqrt{\pi}\kappa r} \tag{2}$$

This relationship was proposed in the 1970s [23] and first used by Nonnenmacher et al. [30] to measure the thermal properties of bulk conductors and of insulating thin films on conducting substrates by thermal scanning probe microscopy. Eq. (2) was later applied to obtain the thermal conductivity of a variety of materials using micro-Raman scattering [14,21,24,25]. This approach assumes that the penetration depth of light ρ in the material, for a given laser wavelength λ, approaches zero and that the sample under study is a semi-infinite half space.

2.2. Numerical simulation

In order to account for the effects of the penetration depth of light and the finite size of the analysed volume, we solved the three-dimensional stationary problem of a micro-Raman thermometry experiment by numerical analysis, based on the finite element method. In this case, the steady state heat equation is solved for a volumetric heat source, which is defined by the Gaussian beam profile within the probed cylindrical volume $V = 4\pi r^2\rho$, according to:

$$-\left(\frac{\partial^2 T}{\partial x^2}+\frac{\partial^2 T}{\partial y^2}+\frac{\partial^2 T}{\partial z^2}\right)\kappa = \frac{2}{\rho}\frac{P_a}{\pi r^2}\exp\left[-2\frac{(x^2+y^2)}{r^2}\right] \tag{3}$$

The incident laser beam is considered to be oriented along the z-direction. The boundary conditions are defined such that overall heat transfer across the top and lateral walls of the sample and the surroundings is zero (adiabatic conditions), while a temperature of $T_\infty = 300$ K is prescribed at the bottom face of the studied specimen (isothermal condition). In particular, we assume perfect thermal contact between the specimen and the sample holder and negligible convection and radiation. Owing to the symmetry of the problem, the simulation is performed in half-volume of the specimen, except when analysing irregular shapes (Section 4.3). It is noteworthy that the measured temperature in the Raman thermometry experiments is a weighted average of the non-uniform temperature distribution across the probed region [21,22]. Thus, to obtain an effective temperature value, the spatially dependent temperature is weighed by the local power density over the above mentioned cylindrical volume, V, the dimensions of which are dictated by the laser profile. The thermal and optical properties [31,32] used for the calculation are given in Table 1.

3. Experimental methods

The micro-Raman shift method was used to measure the thermal conductivity of bulk semiconductors, namely Ge and InP.

Table 1
Material properties used for the FEM model, extracted from Refs. [31,32]. The light penetration depths are at 514.5 nm.

Material	Density (kg/m^3)	Specific heat (J/kg·K)	Penetration depth (nm)
Si	2329	700	664
Ge	5323	310	17
InP	4810	310	88

Moreover, experimental data from Stoib and co-workers [21] for Si were analysed using our simulation. Experiments were performed using a HORIBA Jobin Yvon HR800 Raman spectrometer, equipped with a Peltier-cooled Si-CCD detector and an 1800 l/mm grating. The resolving power of the spectrometer is about 1.2 cm^{-1}, whereas the standard deviation resulting from the fit to the spectra using a Lorentzian function is 0.05 cm^{-1}. An Argon-ion laser operating at 514.5 nm was used simultaneously as heat source and thermometer. The excitation light was focused onto the surface of the specimen using a long working distance objective with a magnifying power of 100x and a numerical aperture of $N.A = 0.6$. The waist size of the nearly-Gaussian spot was measured by scanning the beam across the edge of a gold film deposited on a Si substrate following the procedure reported in Refs. [12,33]. A Gaussian function of the form $I\exp(-x^2/r^2)$, was fitted to the slope of the intensity I of the 1st-order longitudinal and traverse optical (LTO) Raman peak of silicon [34] against the position x, yielding an estimated spot radius of about 0.50 ± 0.07 µm. In-situ reflectance and absorbance measurements were carried out for the complete series of thermal measurements. To do so, an built-in calibrated system, composed of three commercial power meters and a non-polarizing beam splitter, was used to measure the incident (P_i) and reflected power (P_r), from which the reflectance was estimated, according to $R = P_r/P_i$. The transmittance was considered to be negligible since the measured specimens were typically 500µm-thick bulk materials and the light was fully absorbed over this length. The absorbance was determined using the expression $A = (1 - R)$. The temperature dependence of the Raman shift ($d\Delta\omega/dT$) of each sample was determined to calibrate the thermometer. The calibration curves were obtained using a cryostat evacuated to a base pressure of about 1×10^{-3} mbar to control the bath temperature and limit convection losses. Excellent thermal contact between the specimen and the heating plate was ensured by using silver paint. A series of measurements with various excitation laser powers was performed to heat the samples and record the resulting temperature-dependent phonon frequencies as a function of the absorbed power ($d\Delta\omega/dP_a$). The obtained Raman shift dependence was then compared to the calibration curve ($d\Delta\omega/dT$), enabling the estimation of the weighted average temperature rise in the probed volume.

4. Results and discussion

4.1. Validation of the method

The applicability of the Raman shift method was validated using a single-crystal Ge substrate. The shift of the first-order Ge LTO Raman peak [31] as a function of temperature was calibrated by externally heating the sample and performing Raman measurements at an incident power of 0.5 mW to avoid any additional heating of the sample by laser light absorption.

The measured evolution of the Ge peak due to a temperature increase from 343 to 413 K is shown in Fig. 1a, and clearly indicates a red frequency shift due to the variations in the equilibrium position of the atoms and the anharmonicity of the bonds with temperature [35,28,36]. In addition, an increase of the linewidth can be observed, due to the reduced phonon scattering time as the temperature rises. The linear dependence of the Raman shift with temperature is depicted in Fig. 1c and was estimated to be $d\Delta\omega/dT = -0.0160 \pm 0.0003$ cm$^{-1}\cdot$K^{-1} by fitting a Lorentzian function to each spectrum in Fig. 1a, with a mean error of 0.25%. This result is in good agreement with previously reported values of −0.02 [37] and −0.018 cm$^{-1}\cdot$K^{-1} [38]. The Raman shift dependence on power is shown in Fig. 1b. The observed increase in intensity with increasing power is ascribed to the higher number of scattered phonons while the frequency

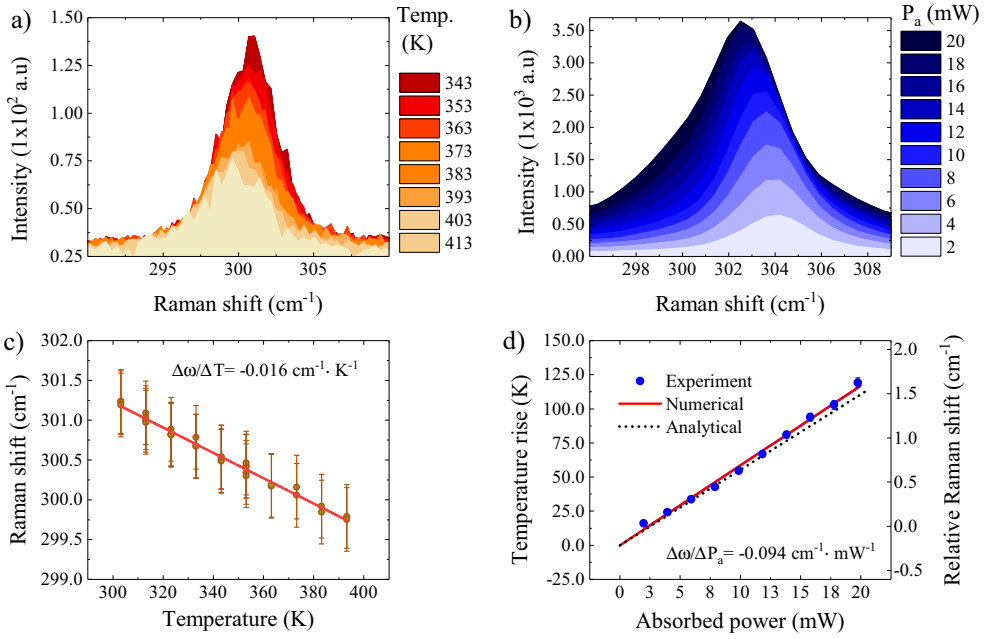

Fig. 1. Raman thermometry of bulk Ge. Raman shift of the first-order Ge peak in response to (a) a temperature increase and (b) to the heating resulting from the power absorbed at the sample surface. (c) Linear dependence of the Ge peak frequency on temperature. (d) Relative Raman shift and corresponding temperature rise as a function of absorbed power.

red-shift is due to light absorption, which ultimately results in thermal expansion due to the induced temperature rise. From these experimental data, we obtain a linear dependence of $d\Delta\omega/dP_a = -0.094 \pm 0.003\ \mathrm{cm^{-1}\cdot mW^{-1}}$, which yields a temperature rise of about 120 K for an absorbed power ranging from 2 to 20 mW, as shown in Fig. 1d. Fitting the obtained values with the finite element model gives a bulk thermal conductivity of 60 W/m·K, in excellent agreement with the value reported by Glassbrenner [39], therefore validating our numerical method. On the other hand, the analytical model (Eq. (2)) yields a thermal conductivity of 56 W/m·K, which represents an underestimate of 7%.

4.2. Effect of light penetration depth

Neglecting the penetration depth of light in the studied material, as assumed in the derivation of Eq. (2) (analytical approximation) is problematic to estimate the temperature rise. Raman thermometry measurements of single crystalline germanium (Ge) and indium phosphide (InP) were performed to investigate this effect further. These samples exhibit a considerable difference in the distance at which the light intensity drops by 1/e, defined as the penetration or skin depth. Moreover, we analysed the experimental values recently reported by Stoib et al. [21] for silicon using a laser at 514.5 nm with a mean radius of 0.73 μm. It is worthnoting that under this experimental conditions, Si has much larger light penetration depth than Ge and InP (Table 1).

The experimental data was interpreted by means of the numerical simulation, varying the penetration depth in each material from 50 to 5000 nm to identify the range of validity of the "shallow absorption" hypothesis used in the analytical approximation.

The experimentally measured temperature rise as a function of absorbed laser power was compared to the theoretical predictions by the numerical (Eq. (3)) and analytical (Eq. (2)) models for Ge, InP and Si [21], as shown in Fig. 2. To interpret these results, the slope of the linear dependence of the temperature rise with the measured absorbed laser power was plotted as a function of the inverse of the penetration depth in Fig. 3.

For an incident laser with wavelength of 514.5 nm, the light penetration depth in Ge is 17 nm, as listed in Table 1. The adequacy of the "shallow absorption" assumption in the analytical model, in the case of Ge, is supported by the relatively good agreement of the FEM and analytical approximations, shown in Fig. 2. In this case,

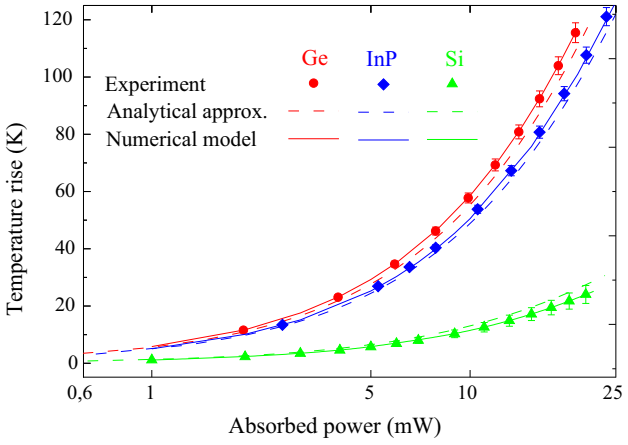

Fig. 2. Temperature rise as a function of the absorbed laser power. Red dots denote the measured bulk Ge, blue diamonds correspond to the bulk InP sample and green triangles to the work of Stoib et al. [21] using Si. Dotted and continuous lines correspond to the analytical and numerical predictions, respectively. (For interpretation of the references to color in this figure legend, the reader is referred to the web version of this article.)

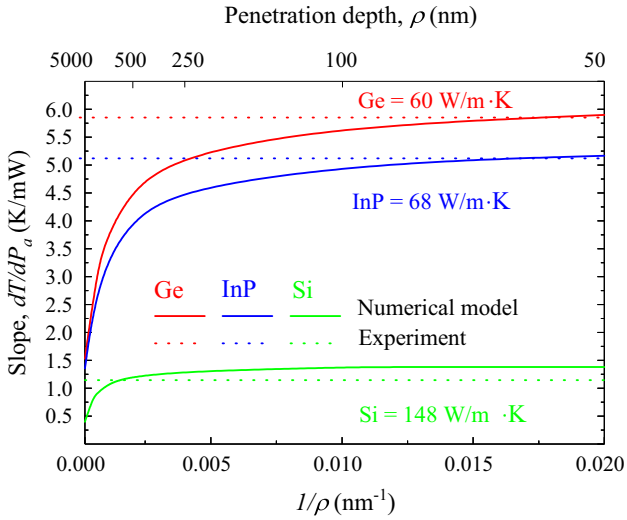

Fig. 3. Slope of the linear dependence of the temperature rise with absorbed laser power as a function of the inverse of the penetration depth. Continuous lines refer to the numerical simulation, where the penetration depth was varied from 50 to 5000 nm. Dashed lines denote the measured slope dT/dP_a for bulk Ge (red), InP (blue) and Si (green) [21]. (For interpretation of the references to color in this figure legend, the reader is referred to the web version of this article.)

the laser spot radius of about 0.50 ± 0.07 μm is more than 20 times larger than the penetration depth ($r \gg \rho$), with a ratio of light penetration depth to spot radius of $\rho/r \approx 0.03$.

Similarly, as shown in Fig. 2, there is a relative good agreement between the experiment, the analytical approximation and the numerical model, for single-crystalline InP ($\rho = 88$ nm at 514.5 nm).

The value obtained for the dependence of the InP transverse optical phonons on temperature was $d\Delta\omega/dT = -0.0180 \pm 0.0020\ \mathrm{cm^{-1}\cdot K^{-1}}$, which is consistent with the linear relation of $-0.017\ \mathrm{cm^{-1}\cdot K^{-1}}$ reported by Irmer and co-workers [40]. The temperature rise shown in Fig. 2, was calculated using the measured absorbed power dependence of the Raman shift of $d\Delta\omega/dP_a = -0.091 \pm 0.004\ \mathrm{cm^{-1}\cdot mW^{-1}}$ for the same phonon mode. In this case, the obtained thermal conductivity was 68 and 65 W/m·K from the FEM and analytical solutions, respectively.

As with Ge, the FEM result matches the generally accepted value of thermal conductivity for bulk InP [41], while the analytical approximation underestimates the temperature rise, predicting a thermal conductivity that is 5% smaller than the reference value. This result suggests that the "shallow absorption" hypothesis used in the analytical model is also fulfilled in the case of InP, where the ratio of light penetration depth to spot radius is of $\rho/r \approx 0.2$. However, for materials where this ratio is higher, such as Si, the analytical approximation results in the temperature rise overestimate, as shown in Fig. 2.

By comparing the numerical results of dT/dP_a as a function of ρ (solid lines in Fig. 3) to the measured slopes (dashed lines in Fig. 3) within a 10% error range, we deduced the absorption conditions that limit the use of the analytical model (Eq. (2)). In this manner, we found that the penetration depth of light in the studied material should be smaller than $1/2r$ to achieve measurement errors below 10% using Eq. (2) ($\rho/r < 0.5$). Under these conditions, the assumption of "shallow absorption" is partially fulfilled and the analytical approximation predicts a thermal conductivity value with an error below 10%.

These modelling results are validated by Raman thermometry experiments, since Eq. (2) predicts the thermal conductivity of Ge and InP, which have a penetration depth shorter than $1/2r$ at the used laser wavelength, with an error below 10%.

However, in the case of Si, the penetration depth of 514 nm light is much larger (664 nm). Recently, Stoib et al. [21] reported experimental values of the dependence of the first order peak on temperature and absorbed power, which were $d\Delta\omega/dT = -0.021\ \mathrm{cm^{-1}\cdot K^{-1}}$ and $d\Delta\omega/dP_a = -0.025\ \mathrm{cm^{-1}\cdot mW^{-1}}$, respectively. Using these parameters, the thermal conductivity obtained from the analytical and FEM models is 168 and 148 W/mK, respectively. In this case, the temperature rise in the experiment is overestimated by the analytic model, leading to an overestimation of the thermal conductivity by as much as 13%. The main reason is that the ratio of penetration depth to spot radius is much larger than 0.5 ($\rho/r = 0.91$), and therefore the analytical approach fails to describe the diffusion of heat toward the rest of the material throughout the effective volume defined by the laser profile. This effect in Si is illustrated in Fig. 3, where the curve of the slope dT/dP_a as a function of the inverse of the penetration depth ρ, does not converge to the experimental result of $dT/dP_a = 1.14$ K/mW for very shallow penetration depth values.

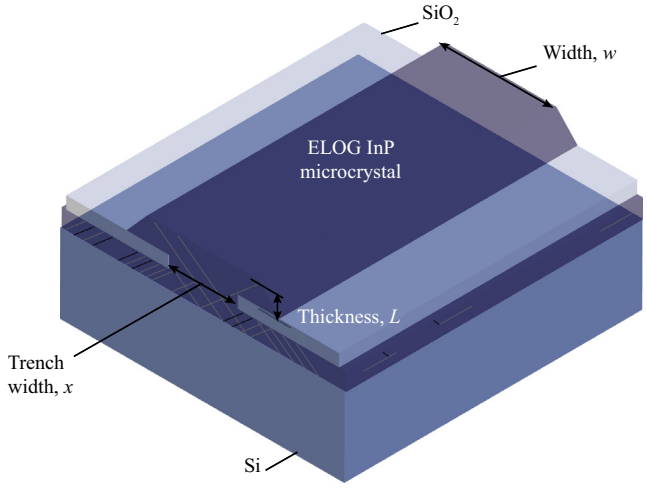

Fig. 4. Schematic illustration of the investigated samples obtained by heteroepitaxial growth of InP on Si using the ELOG technique, and described in Table 2. (For interpretation of the references to color in this figure legend, the reader is referred to the web version of this article.)

4.3. Effect of finite sample size

The influence of finite sample dimensions on the deduction of the temperature rise can also lead to significant measurement errors. In this context, microcrystals of InP grown by epitaxial lateral overgrowth (ELOG) are excellent candidates to study the effect of sample size. In the ELOG method, InP is laterally grown from trenches in a mask deposited on a defect-rich InP seed layer grown on a Si substrate [42]. The mask between the trenches acts as a filter for defects and affects the crystal growth, thus defining the dimensions of the microcrystals. Consequently, crystals grown through smaller trenches are thinner and narrower than those grown through larger trenches [43,44]. We investigated the effect of finite sample size by analysing two different microcrystals of InP grown directly on Si through 250 and 400 nm wide trenches [33]. A schematic representation of the microcrystal samples is depicted in Fig. 4 and their dimensions are listed in Table 2.

The temperature rise as a function of absorbed power in both samples is shown in Fig. 5a. Scanning electron micrographs (SEM) and the modelled geometries for the crystals 1 and 2 are shown in Fig. 5 b, d and c, e, respectively.

The thermal conductivity predicted by the FEM model for the larger sample (crystal 2) is 68 W/m·K, which is the accepted reference value for monocrystalline bulk InP, while the analytical model yields 46 W/m·K. The finite size of the crystal in relation to the " semi-infinite-medium" approximation, implies that the heat generated by the laser diffuses through a smaller volume, therefore rising the effective temperature of the probed region. Since the analytical model does not consider the surfaces bounding the volume, the temperature rise is seriously underestimated, resulting in an error of 32%.

On the other hand, for the smaller sample (crystal 1), a larger temperature rise was measured as expected. The thermal conductivity was found to be 31 (FEM) and 22 W/m·K (analytical solution). The reduction of the thermal conductivity with respect to

Table 2
Dimensions of InP microcrystals.

Sample	Trench width, x (nm)	Thickness, L (μm)	Width, w (μm)	Volume, V_{InP} (μm^3)
Crystal 1	250	1.5	4	150
Crystal 2	400	5	14	4500

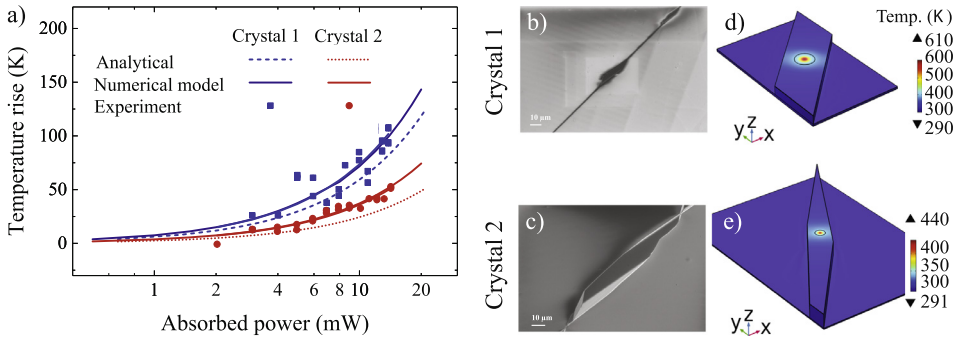

Fig. 5. Comparison between the crystals described in Table 2. (a) Experimental and the modelled values of the temperature rise as a function of power absorbed for samples in Table 2. Symbols refer to the experimental data points while continuous and dashed lines correspond to the FEM and analytical solutions, respectively. (b) and (c) SEM micrographs and (d) and (e) corresponding modelled geometries and temperature fields for the two crystals, respectively.

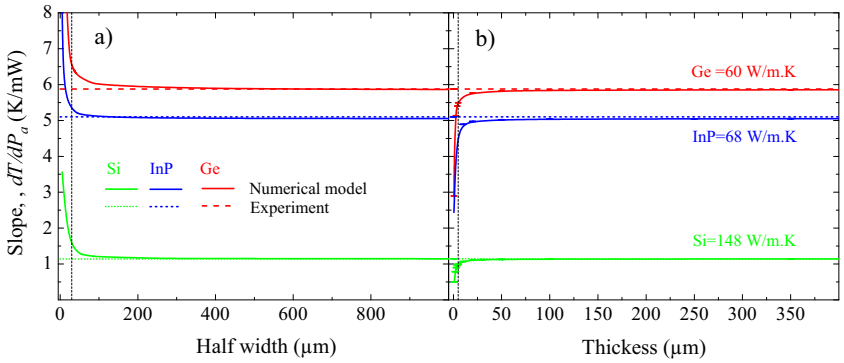

Fig. 6. Slope of the linear dependence of the temperature rise with absorbed laser power as a function of the (a) half width and (b) the thickness of the sample. Continuous lines refer to the numerical simulation and the dashed lines denote the measured slope dT/dP_a for bulk Ge (red), InP (blue) and Si (green) [21]. (For interpretation of the references to color in this figure legend, the reader is referred to the web version of this article.)

the bulk value for the smaller InP microcrystal could result from phonon scattering at stacking faults close to the interface between the ELOG InP and the SiO_2 mask [45,33]. Furthermore, the use of the assumption of a "semi-infinite-medium" in the analytical model leads to an underestimate of the temperature rise, and therefore the predicted thermal conductivity drops by 29%.

From the results obtained using the numerical model for the three materials studied here, we found that finite size effects depend on the adiabatic or isothermal nature of the boundary conditions. The dependence of dT/dP_a on the half width and thickness of the samples are shown in Fig. 6a and b, respectively.

In Fig. 6a and b, we observe that, in the case of microcrystals, to assume an infinite thickness (Eq. (2)) leads to an overestimate of the temperature rise, while considering an infinite width yields to an underestimate. Of these two parameters, the adiabatic lateral surfaces have a predominant role (Fig. 6a). We found that the semi-infinite substrate approximation is fulfilled if the half width of the sample is at least 100 times larger than the spot radius, for thermal conductivity predictions with errors below 10% using Eq. (2). On the other hand, the thickness of the studied specimen should be at least 10 times bigger than the spot radius to fulfill this assumption and to obtain results within 10% error. In this study, the thickness and width of crystal 1 and 2 are comparable to the laser beam diameter, and thus the assumption of the "semi-infinite-medium" is not fulfilled under these experimental conditions, explaining the high measurement error yielded by the analytical formula.

5. Conclusions

We developed a finite-element based numerical simulation of the heating of bulk and microscale mesa-like samples induced by a Gaussian laser beam. We analysed the errors associated with Raman thermometry measurements emerging from the assumptions in the heat conduction models used to extract the thermal conductivity, such as the effects of the light penetration depth and finite sample size. By comparing our numerical model with the simplified analytical solution for the case of laser heating of a semi-infinite solid, we obtained the range of applicability of such conditions. We found that the ratio between light penetration depth to laser spot radius should be smaller than 0.5 to achieve measurement errors below 10% when using the assumption of strong absorption at the surface in the analytical approximation. Furthermore, we obtained that the "semi-infinite substrate thickness hypothesis" is valid and yields results with less than 10% error if the ratio of spot radius to sample thickness is smaller than 0.1. On the other hand, the "semi-infinite medium approximation" is fulfilled if the sample half width is at least 100 times larger than the spot radius. This study is a powerful tool to estimate errors when analysing Raman thermometry measurements by means of analytical formulae, considering sample geometry and light absorption conditions to estimate the thermal conductivity of bulk materials.

Acknowledgments

JJF and CMST acknowledge the Swedish Research Council VR (349-2007-8664 and 2014-5100) and the Linnaeus Center in Advanced Optics and Photonics for financial support. CMST and ECA acknowledge support from the Spanish MINECO and the Catalan AGAUR (FIS2015-70862-P and CSD2010-00044). JJF is especially grateful to Dr. M. Sledzinska and Dr. B Graczykowski for discussions and assistance with the Raman measurements and simulations. JJF thanks Profs. S. Anand and S. Lourdudoss, and Mr. A. Abedin, for providing the bulk and microcrystal samples. ICN2 acknowledges support from the Severo Ochoa Program (MINECO, Grant SEV-2013-0295) and funding from the CERCA Programme/Generalitat de Catalunya.

References

[1] T. Borca-Tasciuc, G. Chen, Experimental techniques for thin-film thermal conductivity characterization, in: T.M. Tritt (Ed.), Thermal Conductivity, Springer, US, 2004, pp. 205–237, https://doi.org/10.1007/b136496.
[2] J. Jaramillo-Fernandez, Tuning the Thermal Conductivity of Polycrystalline Films via Multiscale Structural Defects and Strain (Ph.D. thesis), Ecole Centrale Paris, 2015.
[3] D. Zhao, X. Qian, X. Gu, S.A. Jajja, R. Yang, Measurement techniques for thermal conductivity and interfacial thermal conductance of bulk and thin film materials, J. Electron. Packag. 138 (4) (2016) 0408021–04080219, https://doi.org/10.1115/1.4034605. <http://electronicpackaging.asmedigitalcollection.asme.org/article.aspx?doi=10.1115/1.4034605>.
[4] D.G. Cahill, Thermal conductivity measurement from 30 to 750 K: the 3ω method, Rev. Sci. Instrum. 61 (2) (1990) 802–808, https://doi.org/10.1063/1.1141498. <http://scitation.aip.org/content/aip/journal/rsi/61/2/10.1063/1.1141498>.
[5] D.G. Cahill, Analysis of heat flow in layered structures for time-domain thermoreflectance, Rev. Sci. Instrum. 75 (12) (2004) 5119–5122, https://doi.org/10.1063/1.1819431. http://aip.scitation.org/doi/10.1063/1.1819431.
[6] A.J. Schmidt, R. Cheaito, M. Chiesa, A frequency-domain thermoreflectance method for the characterization of thermal properties, Rev. Sci. Instrum. 80 (9) (2009) 0949011–0949016, https://doi.org/10.1063/1.3212673. <http://aip.scitation.org/doi/10.1063/1.3212673>.
[7] C.B. Saltonstall, J. Serrano, P.M. Norris, P.E. Hopkins, T.E. Beechem, Single element Raman thermometry, Rev. Sci. Instrum. 84 (6) (2013) 0649031–0649037, https://doi.org/10.1063/1.4810850. <http://aip.scitation.org/doi/10.1063/1.4810850>.
[8] I. Hatta, Y. Sasuga, R. Kato, A. Maesono, Thermal diffusivity measurement of thin films by means of an AC calorimetric method, Rev. Sci. Instrum. 56 (8) (1985) 1643–1647, https://doi.org/10.1063/1.1138117. <http://aip.scitation.org/doi/10.1063/1.1138117>.
[9] O. Bourgeois, E. André, C. Macovei, J. Chaussy, Liquid nitrogen to room-temperature thermometry using niobium nitride thin films, Rev. Sci. Instrum. 77 (12) (2006) 1261081–1261083, https://doi.org/10.1063/1.2403934. <http://aip.scitation.org/doi/10.1063/1.2403934>.

[10] W. Zhao, W. Chen, Y. Yue, S. Wu, In-situ two-step Raman thermometry for thermal characterization of monolayer graphene interface material, Appl. Therm. Eng. 113 (2017) 481–489, https://doi.org/10.1016/j.applthermaleng.2016.11.063. <http://www.sciencedirect.com/science/article/pii/S1359431116331441>.
[11] A.A. Balandin, Thermal properties of graphene and nanostructured carbon materials, Nat. Mater. 10 (8) (2011) 569–581, https://doi.org/10.1038/nmat3064.
[12] W. Cai, A.L. Moore, Y. Zhu, X. Li, S. Chen, L. Shi, R.S. Ruoff, Thermal transport in suspended and supported monolayer graphene grown by chemical vapor deposition, Nano Lett. 10 (5) (2010) 1645–1651, https://doi.org/10.1021/nl9041966.
[13] S. Périchon, V. Lysenko, P. Roussel, B. Remaki, B. Champagnon, D. Barbier, P. Pinard, Technology and micro-Raman characterization of thick meso-porous silicon layers for thermal effect microsystems, Sens. Actuators, A 85 (1) (2000) 335–339, https://doi.org/10.1016/S0924-4247(00)00327-7.
[14] S. Huang, X. Ruan, J. Zou, X. Fu, H. Yang, Thermal conductivity measurement of submicrometer-scale silicon dioxide films by an extended micro-Raman method, Microsyst. Technol. 15 (6) (2009) 837–842, https://doi.org/10.1007/s00542-009-0824-3.
[15] G.S. Doerk, C. Carraro, R. Maboudian, Single nanowire thermal conductivity measurements by Raman thermography, ACS Nano 4 (8) (2010) 4908–4914, https://doi.org/10.1021/nn1012429.
[16] Q. Li, C. Liu, X. Wang, S. Fan, Measuring the thermal conductivity of individual carbon nanotubes by the Raman shift method., Nanotechnology 20 (14) (2009) 1457021–14570215, https://doi.org/10.1088/0957-4484/20/14/145702.
[17] J.U. Lee, D. Yoon, H. Kim, S.W. Lee, H. Cheong, Thermal conductivity of suspended pristine graphene measured by Raman spectroscopy, Phys. Rev. B 83 (8) (2011) 0814191–0814194, https://doi.org/10.1103/PhysRevB.83.081419.
[18] E. Chávez-Ángel, J.S. Reparaz, J. Gomis-Bresco, M.R. Wagner, J. Cuffe, B. Graczykowski, A. Shchepetov, H. Jiang, M. Prunnila, J. Ahopelto, F. Alzina, C.M. Sotomayor Torres, Reduction of the thermal conductivity in free-standing silicon nano-membranes investigated by non-invasive Raman thermometry, APL Mater. 2 (2014) 0121131–0121136, https://doi.org/10.1063/1.4861796.
[19] J. Jaramillo-Fernandez, J. Ordonez-Miranda, W. Kassem, E. Oilier, S. Volz, Thermal conductivity of polycrystalline aluminum nitride films: effects of the microstructure, interfacial thermal resistance and local oxidation, in: Proceedings of the 21st International Workshop on Thermal Investigations of ICs and Systems (THERMINIC), 2015, pp. 1–6. https://doi.org/10.1109/THERMINIC.2015.7389602. <http://ieeexplore.ieee.org/lpdocs/epic03/wrapper.htm?arnumber=7389602>.
[20] J.S. Reparaz, E. Chavez-Angel, M.R. Wagner, B. Graczykowski, F. Alzina, C.M. Sotomayor Torres, A novel contactless technique for thermal field mapping and thermal conductivity determination: two-laser Raman thermometry, Rev. Sci. Instrum. 85 (2014) 0349011–0349015, https://doi.org/10.1063/1.4867166.
[21] B. Stoib, S. Filser, J. Stötzel, A. Greppmair, N. Petermann, H. Wiggers, G. Schierning, M. Stutzmann, M.S. Brandt, Spatially resolved determination of thermal conductivity by Raman spectroscopy, Semicond. Sci. Technol. 29 (2014) 1240051–12400513, https://doi.org/10.1088/0268-1242/29/12/124005.
[22] J. Očenášek, J. Voldich, Raman thermometry: effective temperature of the nonuniform temperature field induced by a Gaussian laser, J. Appl. Phys. 118 (23) (2015) 2331041–2331045, https://doi.org/10.1063/1.4937904.
[23] M. Lax, Temperature rise induced by a laser beam, J. Appl. Phys. 48 (9) (1977) 3919–3924, https://doi.org/10.1063/1.324265.
[24] V. Lysenko, S. Perichon, B. Remaki, D. Barbier, B. Champagnon, Thermal conductivity of thick meso-porous silicon layers by micro-Raman scattering, J. Appl. Phys. 86 (12) (1999) 6841–6846, https://doi.org/10.1063/1.371760, http://link.aip.org/link/JAPIAU/v86/i12/p6841/s1&Agg=doi\nhttp://ieeexplore.ieee.org/xpl/articleDetails.jsp?arnumber=5024256\nhttp://scitation.aip.org/content/aip/journal/jap/86/12/10.1063/1.371760.
[25] S. Perichon, V. Lysenko, B. Remaki, D. Barbier, B. Champagnon, Measurement of porous silicon thermal conductivity by micro-Raman scattering, J. Appl. Phys. 86 (8) (1999) 4700, https://doi.org/10.1063/1.371424. <http://scitation.aip.org/content/aip/journal/jap/86/8/10.1063/1.371424>.
[26] C. Glynn, K.-M. Jones, V. Mogili, W. McSweeney, C. O'Dwyer, The nature of silicon nanowire roughness and thermal conductivity suppression by phonon scattering mechanisms, ECS J. Solid State Sci. Technol. 6 (3) (2017) N3029–N3035, https://doi.org/10.1149/2.0071703jss.
[27] T. Beechem, L. Yates, S. Graham, Invited review article: error and uncertainty in Raman thermal conductivity measurements, Rev. Sci. Instrum. 86 (4) (2015) 0411011–04110111, https://doi.org/10.1063/1.4918623.
[28] T.E. Beechem, J.R. Serrano, Raman thermometry of microdevices: comparing methods to minimize error, Spectros.: Solut. Mater. Anal. 26 (11) (2011) 36–44.
[29] H. Carslaw, J. Jaeger, Conduction of Heat in Solids, Oxford University Press, Oxford, 1959.
[30] M. Nonnenmacher, H.K. Wickramasinghe, Scanning probe microscopy of thermal conductivity and subsurface properties, Appl. Phys. Lett. 61 (2) (1992) 168–170, https://doi.org/10.1063/1.108207.
[31] O. Madelung, Semiconductors: Data Handbook, Springer, Berlin, Heidelberg, 2012, https://doi.org/10.1007/978-3-642-18865-7_1.
[32] D.E. Aspnes, A.A. Studna, Dielectric functions and optical parameters of Si, Ge, GaP, GaAs, GaSb, InP, InAs, and InSb from 1.5 to 6.0 eV, Phys. Rev. B 27 (2) (1983) 985–1009.
[33] J. Jaramillo-Fernandez, E. Chavez-Angel, R. Sanatinia, H. Kataria, S. Anand, S. Lourdudoss, C.M. Sotomayor-Torres, Thermal conductivity of epitaxially grown InP: experiment and simulation, CrystEngComm 19 (14) (2017) 1879–1887, https://doi.org/10.1039/C6CE02642G.
[34] R. Tubino, L. Piseri, G. Zerbi, Lattice dynamics and spectroscopic properties by a valence force potential of diamondlike crystals: C, Si, Ge, and Sn, J. Chem. Phys. 56 (3) (1972) 1022–1039, https://doi.org/10.1063/1.1677264.
[35] D. Tuschel, Raman thermometry, Spectros.: Solut. Mater. Anal. 31 (12) (2016) 8–13.
[36] G. Lucazeau, Effect of pressure and temperature on Raman spectra of solids: anharmonicity, J. Raman Spectrosc. 4 (2003) 478–496, https://doi.org/10.1002/jrs.1027.
[37] J. Menendez, M. Cardona, Temperature dependence of the first-order Raman scattering by phonons in Si, Ge, and α Sn: anharmonic effects, Phys. Rev. B 29 (4) (1984) 2051–2059.
[38] H.H. Burke, I.P. Herman, Temperature dependence of Raman scattering in Ge 1 x Si x alloys, Phys. Rev. B 48 (20) (1993) 16–24.
[39] C. Glassbrenner, G. Slack, Thermal conductivity of silicon and germanium from 3 K to the melting point, Phys. Rev. 134 (4A) (1964) A1058–A1069. <http://journals.aps.org/pr/abstract/10.1103/PhysRev.134.A105>.
[40] G. Irmer, M. Wenzel, J. Monecke, The temperature-dependence of the LO and TO phonons in GaAs and InP, Phys. Status Solidi (B) 195 (85) (1996) 85–95.
[41] P.D. Maycock, Thermal conductivity of silicon, germanium, III-V compounds and III-V alloys, Solid-State Electron. 10 (3) (1967) 161–168.
[42] H. Kataria, W. Metaferia, C. Junesand, C. Zhang, N. Julian, J.E. Bowers, Simple epitaxial lateral overgrowth process as a strategy for photonic integration on silicon, IEEE J. Sel. Top. Quant. Electron. 20 (4) (2014) 380–386.
[43] C. Junesand, H. Kataria, W. Metaferia, N. Julian, Y.-t. Sun, J. Bowers, G. Pozina, L. Hultman, Study of planar defect filtering in InP grown on Si by epitaxial lateral overgrowth, Opt. Mater. Exp. 3 (11) (2013) 1960–1973, https://doi.org/10.1364/OME.3.001960.
[44] J. Jaramillo-Fernandez, J. Ordonez-Miranda, E. Ollier, R. Sanatinia, H. Kataria, E. Chavez-Angel, S. Volz, C.M. Sotomayor Torres, Tuning of heat transport across thin films of polycristalline AlN via multiscale structural defects, ECS Trans. 69 (9) (2015) 53–64, https://doi.org/10.1149/06909.0053ecst.
[45] J. Jaramillo-Fernandez, J. Ordonez-Miranda, E. Ollier, S. Volz, Tunable thermal conductivity of thin films of polycrystalline AlN by structural inhomogeneity and interfacial oxidation., PCCP 17 (12) (2015) 8125–8137, https://doi.org/10.1039/c4cp05838k. <http://www.ncbi.nlm.nih.gov/pubmed/25729791>.